AIP | Review of Scientific Instruments

A multichord spectrometer using an 8×8 anode photomultiplier(a)

P. G. Carolan and R. O'Connell

Citation: Rev. Sci. Instrum. 66, 1184 (1995); doi: 10.1063/1.1146003
View online: http://dx.doi.org/10.1063/1.1146003
View Table of Contents: http://rsi.aip.org/resource/1/RSINAK/v66/i2
Published by the American Institute of Physics.

Related Articles

Fourier transform infrared absorption spectroscopy characterization of gaseous atmospheric pressure plasmas with 2 mm spatial resolution
Rev. Sci. Instrum. 83, 103508 (2012)

Kr II laser-induced fluorescence for measuring plasma acceleration
Rev. Sci. Instrum. 83, 103111 (2012)

Laser schlieren deflectometry for temperature analysis of filamentary non-thermal atmospheric pressure plasma
Rev. Sci. Instrum. 83, 103506 (2012)

Reconstruction of polar magnetic field from single axis tomography of Faraday rotation in plasmas
Phys. Plasmas 19, 103107 (2012)

Study of the plasma wave excited by intense femtosecond laser pulses in a dielectric capillary
Phys. Plasmas 19, 093121 (2012)

Additional information on Rev. Sci. Instrum.

Journal Homepage: http://rsi.aip.org
Journal Information: http://rsi.aip.org/about/about_the_journal
Top downloads: http://rsi.aip.org/features/most_downloaded
Information for Authors: http://rsi.aip.org/authors

ADVERTISEMENT

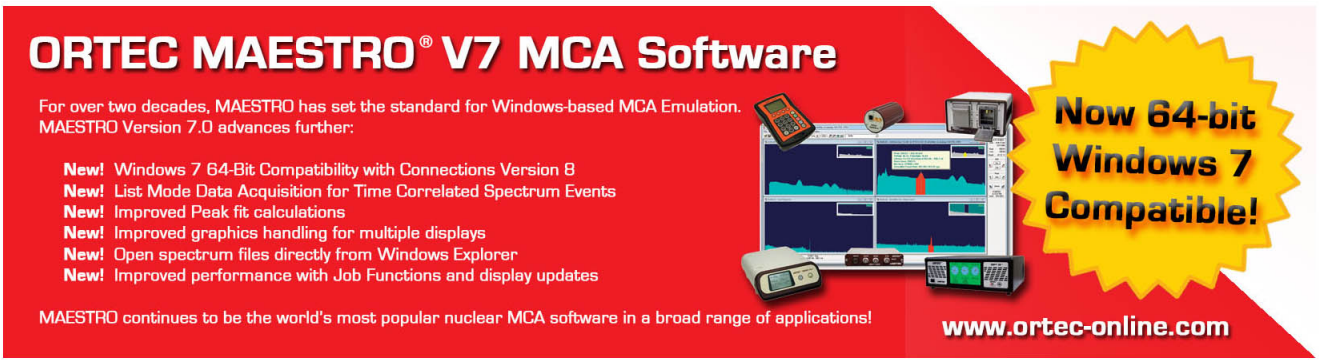

A multichord spectrometer using an 8×8 anode photomultiplier[a)]

P. G. Carolan and R. O'Connell[b)]
UKAEA Government Division (UKAEA/Euratom Fusion Association), Culham, Abingdon, Oxon, OX14 3DB, United Kingdom

(Presented on 10 May 1994)

A multianode photomultiplier (8×8 anodes of 2.5×2.5 mm^2) is used to detect a collection of spectra in a high dispersion *echelle* spectrometer. A cylindrical lens is placed at the output slit to increase the dispersion at the photomultiplier. The cross talk between adjacent spectra is non-negligible (although <5%), resulting in some interspectral distortion. This is removed by solving a system of simultaneous equations, one for each channel, obtained from the measured cross-talk coefficients. The spectrometer has been used on the COMPASS-D tokamak to measure ion temperatures and fluid velocities. © *1995 American Institute of Physics.*

I. INTRODUCTION

The behavior of plasma rotation has been of interest in magnetic confinement plasmas almost since their conception.[1] Frictional force balance between the various particle species was used[2] in interpreting some of the early Doppler-effect results, especially in relating impurities to the background ions, but the role of radial electric field was also appreciated and indeed the Doppler-effect results were used to diagnose the internal electric fields in a plasma.[3] Momentum confinement[4] and the effects of error fields on the plasma rotation[5–7] were also studied and, more recently, the role of radial electric field profiles in *L*- to *H*-mode transitions.[8–10] There are many plasma (e.g., poloidal viscous damping[11]) and atomic physics features (e.g., elapse time from excitation to decay[9]) which have to be considered in interpreting the observations, while taking due account of instrumental effects (e.g., spatial cross talk[12]). All of these considerations place great demands on the design of the apparatus, detector specifications, and analysis software.

Many of the changes to the fluid velocities in a tokamak plasma can occur over small extents in the spatial and temporal domains. In using Doppler-effect spectroscopy this requires multichannel spectrum detectors at many spatial positions and with very fast time resolution. Here we avail of an *echelle* grating diffractor,[13] providing large solid angles of collected light. Dispersion in the detector plane is further enhanced by using a cylindrical lens at the output slit. A multispectrum fast response system is provided by incorporating a two-dimensional anode array in a single photomultiplier. The cross talk is negligible beyond neighboring pixels and so allowing the reliable use of an algebraic method of deconvolution. The resulting spectra from the various viewing chords are then analyzed with least-square-fitting techniques which include the effects of the measured spectral instrument functions.

[a)]The abstract for this paper appears in the Proceedings of the Tenth Topical Conference on High Temperature Plasma Diagnostics in Part II, Rev. Sci. Instrum. **66**, 609 (1995).

[b)]Also at: Dept. of Experimental Physics, University College Dublin, Ireland.

II. DESCRIPTION OF APPARATUS

A. Photomultiplier and electronics

The photomultiplier device used is the Phillips XP4102X 64-channel tube. Nearest-neighbor pixels have less than 5% cross talk and next-nearest neighbors have less than 1% cross talk. Also, if the character of the observed spectra allows the resolution to be reduced, adjacent spectral channels (in the horizontal direction, say) can be hardwired together to increase the signal to noise. The *RC*-smoothed output is amplified with low impedance current preamplifiers which feed into standard voltage amplifiers. In our first proof-of-principle operation the photomultiplier anodes are hardwired to give 24 outputs, i.e., six spectral channels for four different lines of sight. The six spectral channels overspecify the expected Gaussian line profile and so allows the background continuum to be included in the analysis as well as obtaining error bars in the fitting parameters.

The temperature and velocity are all measured with 100 μs time resolution set by the *RC* filtering and the typical available photon fluxes from the boron^{3+} 282 nm spectral line.

B. Optics and spectrometer

Light from many views of the COMPASS-D plasma is conveyed to a remote grating spectrometer via multiple fiber optics (1 mm diameter, high UV transmittance[14] with ~0.2 dB/m losses at 280 nm). The fiber outputs are imaged atop of each other at the input slit of the spectrometer as illustrated in Fig. 1. The beam splitter in the spectrometer allows the dispersed spectrum to be analyzed simultaneously by fast photomultiplier action and the slower, but more detailed, CCD detector array.

To obtain the required high spectral dispersion and light throughput (i.e., *etendu*) a large echelle grating (316 g/mm 20×10 cm^2) replaces a conventional grating in a 1 m Czerny–Turner spectrometer.[13] The dispersion is further enhanced, at the photomultiplier, by placing a 3 mm diameter quartz rod[15] directly at the output slit. Since no imaging is involved there is a smearing of $\approx 1/f \times D$, where $1/f(\approx 1/10)$ is the f number of the spectrometer and $D \approx 25$ mm the distance of the photocathode from the slit. The smearing of ≈2.5 mm diameter is acceptable, in our present arrangement,

 0034-6748/95/66(2)/1184/5/$6.00

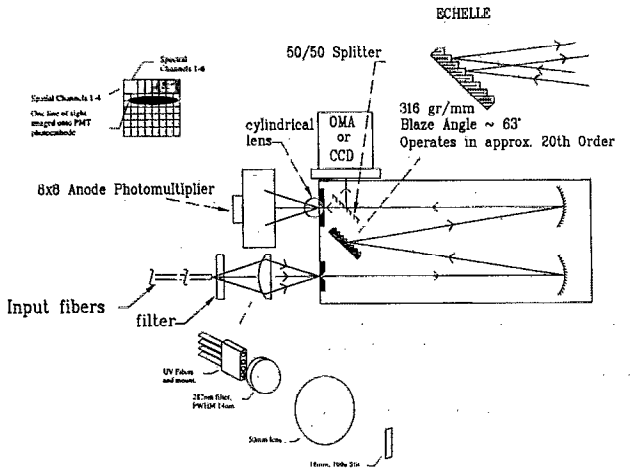

FIG. 1. Schematic of the echelle spectrometer, relay optics from fibers to input slit, and the multianode photomultiplier and cylindrical lens arrangement.

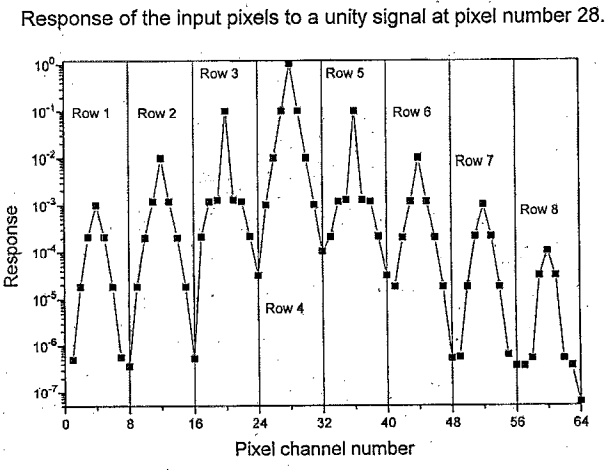

FIG. 3. Deconvolution of a unit signal in a central channel $(m,n=4,4)$ of an 8×8 matrix. All the input channels are assumed to have similar instrument functions described by a 3×3 matrix with values 0.02, 0.1, 0.02; 0.1, 1.0, 0.1; and 0.02, 0.1, 0.02.

for both the spectral instrument function and the vertical cross talk (two vertical anodes, ≈5 mm, are hardwired for each spectral channel). At the wavelengths of current interest for us (282 nm from the $1s2s(S^3)\rightarrow1s2p(P_2^3)$ transition in boron^{3+}) the diffraction order of the echelle is ~20 and the free spectral range is ~15 nm. This allows the use of a relatively high transmittance interference filter[16] with peak transmission of 25% and a FWHM of 14 nm to act as a diffraction order selector.

III. SPECTRAL AND SPATIAL INSTRUMENTAL FUNCTIONS

A. Measurement of spectral instrument functions

The spectral instrument response function of each of the photomultiplier channels (in the horizontal direction, say) is measured using a narrow atomic line spectral source. A single input fiber, representing a line of sight from the plasma, is illuminated and the output of the fiber is imaged at the input slit of the spectrometer. The image of the input slit is swept across the front face of the photomultiplier, each channel acting as an output slit, by rotating the echelle grating. The temporal behavior of each of the channels is converted to a spectral response, or instrument function, by simply applying the grating equation. Successive collection fibers can be illuminated and scanned in this way, giving the response for the photomultiplier (spectral) channels to, essentially, spectral delta-function inputs. Examples of instrument functions from six adjacent spectral channels, occupying two rows of anodes, are illustrated in Fig. 2, where a single input fiber is illuminated. These were taken using a mercury lamp ($\lambda=253.6$ nm). The outermost channels are broader to collect more light at the spectral wings of the Doppler spectrum and is achieved by hardwiring two adjacent anodes.

B. Measurement of spatial instrument functions

In addition to the spectral smearing, arising mainly from the imaging and dispersion properties of the spectrometer,

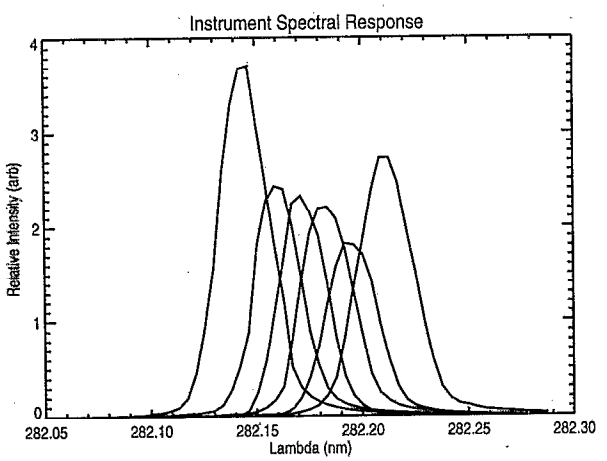

FIG. 2. Measured instrument functions of six spectral channels. These are obtained using a spectral line (Hg, 253.6 nm) and scanning the echelle grating.

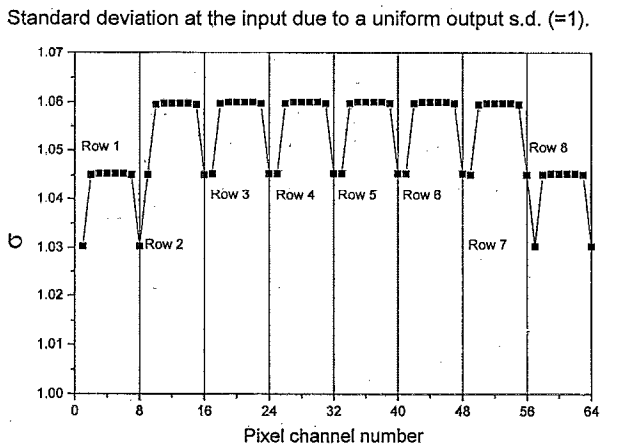

FIG. 4. The standard deviation arising in each of the deconvolved channels due to a uniform standard deviation in the output, or smeared, channels. The same conditions apply as used in Fig. 3.

there is the more direct smearing due to the cross talk in the photomultiplier channels themselves. If there were only a single spatial view of interest, this cross talk would already have been included in the instrument function measurements above which are all that are required in unfolding the data. With more spatial views the observed spectra will have contributions from more than a single view of the plasma. The pixel-to-pixel cross talk is measured by using narrow entrance and exit slits and rotating the grating as before, while illuminating only one fiber at a time. At each channel peak response (almost "top hat" in form), the cross talk is recorded from all the other channels. This method includes all the cross-talk contributions from the optics, spectrometer, and the photomultiplier. Little or no cross talk is observed between nonadjacent pixels. Thus the spatial instrument functions can be represented by a 3×3 matrix for each of the pixels. The table below lists the spot function for a typical channel:

$$\begin{bmatrix} 0 & 0.041 & 0 \\ 0.0163 & 1.0 & 0.0166 \\ 0 & 0.038 & 0 \end{bmatrix}.$$

IV. ALGEBRAIC DECONVOLUTION

A. Principles

The smearing implicit in all experimental data, such as due to the finite resolution of a spectrometer or finite bandwidth of an amplifier, is often conceived as an analog phenomenon and so involving integrals in the mathematical description. However, the problem of smearing can be equally considered in terms of summations of discrete values rather than continuous integration, especially when analyzing experimental data. This approach easily allows for each data channel to have a unique instrument function. The basic idea is to describe a smearing problem, perhaps multidimensional, in terms of a set of linear equations, one equation for each detector channel. The number of terms in each equation is just the number of input channel locations that contribute to that particular detector channel due to smearing. However, in contrast to other approximate means of deconvolution, this approach requires that there is an equal number of equations to unknowns, represented here by the input intensity channels. Thus the effect of smearing must not extend beyond the number of data channels, or that the intensity values outside this range are known (e.g.,=0). This can be achieved in prac-

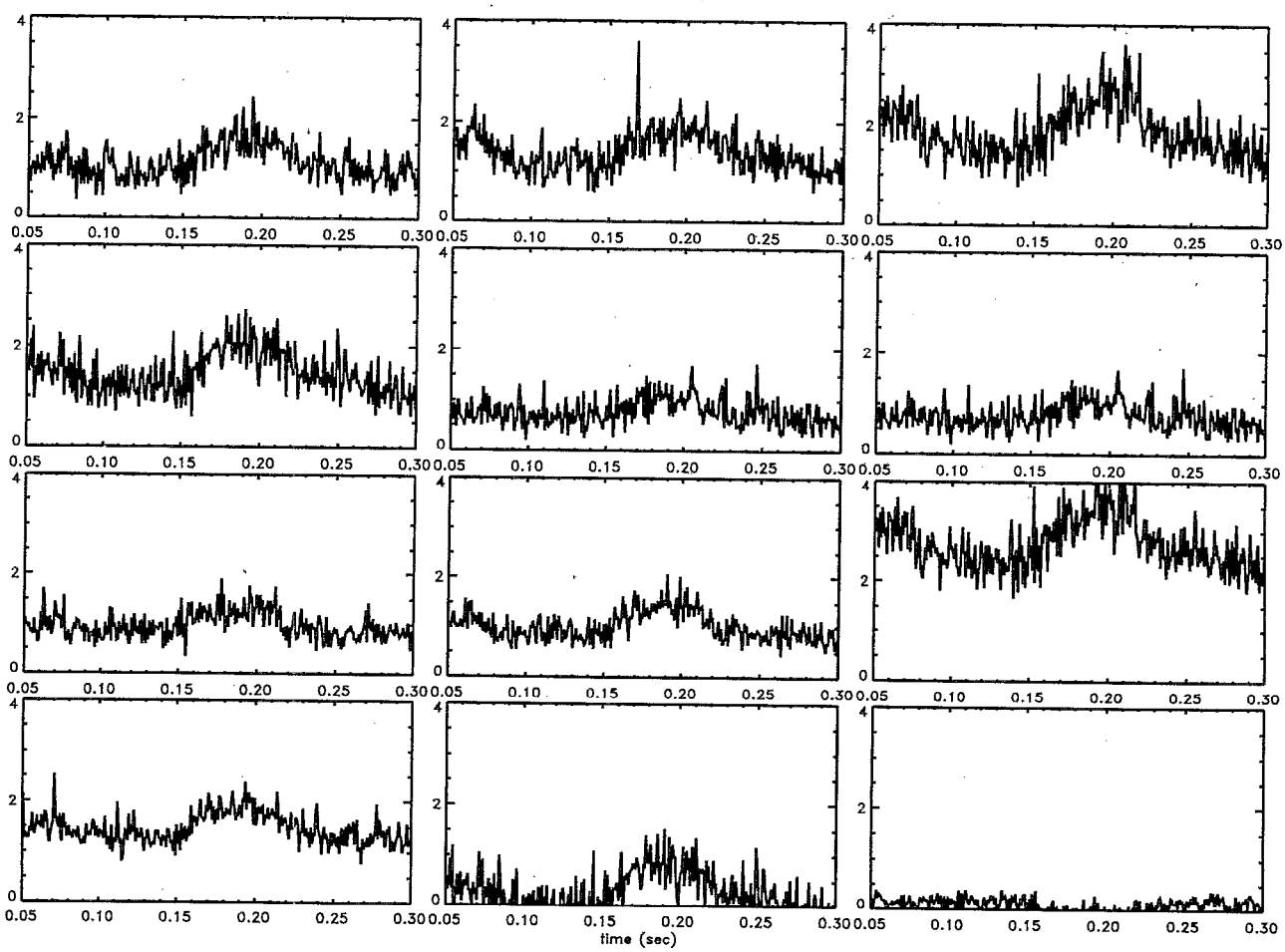

FIG. 5. Typical wave forms of raw data of the spectral channels obtained from two vertical viewing chords, of the COMPASS-D plasma. The six spectral channels go from left to right for the two chords of data shown here.

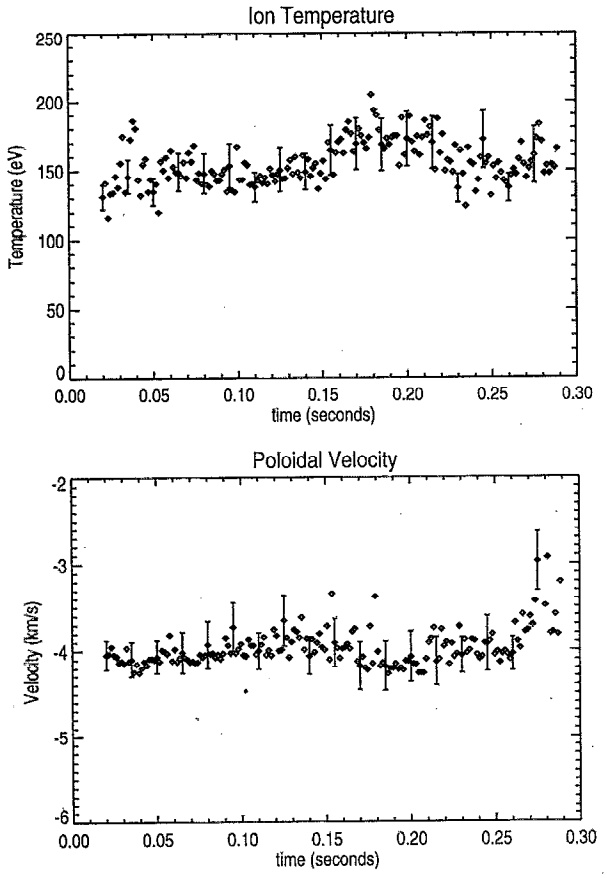

FIG. 6. Analysis of the data shown in Fig. 5 (top chord) in terms of line-intensity-averaged ion temperatures (boron^{3+}) and relative velocity using the measured instrument functions in Fig. 2, and incorporating the calculated Zeeman splitting and after removing the effects of detector cross talk.

tice by masking at the input position. Deconvolution then consists of solving the simultaneous equations for the input intensities, given the measured instrument functions and signal data.

To illustrate the principles, the algebra is restricted here to two spatial dimensions, appropriate to our present needs. Suppose we have an $M\times N$ matrix of detector signals, each represented by S_{mn}, with a corresponding array of image intensities I_{mn} that we wish to determine. Each input coordinate, (m,n), will have an associated instrumental matrix, of size $J\times K$, whose elements are represented here by a_{mnjk}.

The dimensionality of all the matrices may be reduced by joining up the rows, say, in sequence. (A similar process can obviously be used for higher dimensions.) The new matrix elements are represented by $\mathscr{S}_\nu(\equiv S_{mn})$, $\mathscr{I}_\nu(\equiv I_{mn})$, and $\alpha_{\nu jk}$ $(\equiv a_{mnjk})$, where $\nu=(m-1)N+n$ and $1\leqslant\nu\leqslant M\times N$. The relationship between the column vectors $\mathscr{S}$ and $\mathscr{I}$ is given by $\mathsf{A}\times\mathscr{I}=\mathscr{S}$, where A is of size $(M\times N)^2$. It can be shown that the A matrix elements $A_{\mu\nu}$ are obtained from the instrumental matrix elements; viz. $A_{\mu\nu}=\alpha_{\nu jk}$, where j,k is the solution pair to the integer equation:

$$jN+k=(\mu-\nu)+N\,\frac{J+1}{2}+\frac{K+1}{2},$$

with the restrictions of $1\leqslant j\leqslant J$ and $1\leqslant k\leqslant K$ (J and K are assumed here to be odd). There is at most one solution pair, and when there is none, then $A_{\mu\nu}=0$.

To obtain $\mathscr{I}_\nu$, (and hence I_{mn}, the input intensities, or deconvolved signal), it only remains to obtain the matrix inversion of A. Since the matrix depends on the instrument functions alone then this operation need be performed but once for a series of data sets obtained with the same instrument functions.

B. Statistical effects

Since the solutions of the set of simultaneous equations are given by a matrix multiplication of the signal data channels (i.e., $\mathscr{I}=\mathsf{A}^{-1}\times\mathscr{S}$), a statistical variation of $\delta\mathscr{S}$ in the output signal vector $\mathscr{S}$ will have a corresponding change of $\delta\mathscr{I}$ in the input intensity vector $\mathscr{I}$, given by: $\delta\mathscr{I}=\mathsf{A}^{-1}\times\delta\mathscr{S}$. It is clear that errors in one of the elements in $\mathscr{S}$ will influence all of the channels in $\mathscr{I}$. The effects of these errors will obviously depend on the type and magnitude of the signal noise. Let the standard deviation at a signal channel be represented by ${}_s\sigma_\nu$ and the corresponding solution be given by the vector ${}_i\boldsymbol{\sigma}_\nu$. The absolute value of each of the elements in ${}_i\boldsymbol{\sigma}_\nu$, say, ${}_i\sigma_{\mu\nu}$, will be the standard deviation at that input channel due to the statistical variations in the νth output channel. An example of an input intensity profile, or deconvolution profile, arising from a unit signal in only one output channel is shown in Fig. 3. For convenience we have taken absolute values and a one-dimensional plot is used where the response of the pixels is plotted row after row. Here the unit signal was in pixel number 28, almost at the center of the array. All the input channels are assumed to have the same instrument functions described by a 3×3 matrix with values 0.02, 0.1, 0.02; 0.1, 1.0, 0.1; and 0.02, 0.1, 0.02. The instrument functions are truncated at the boundaries defined by the detector matrix (i.e., there is no smearing from domains beyond that defined by the detector boundaries).

The falloff in the deconvolution response from pixel 28, in this case, is a measure of how other channels will be affected by signals in pixel 28. Similar profiles would be obtained from signals appearing individually in all the other channels. If these "signals" are the standard deviations at each of the output channels, then the standard deviation ${}_i\sigma_\mu$ at each of the input channels is the square root of the sum of the squares, obtained from each profile, at each channel. It is straightforward to show that:

$${}_i\sigma_\mu=\left[\sum_{\nu=1}^{M\times N}({}_s\sigma_\mu A_{\mu\nu}^{-1})^2\right]^{1/2}.$$

A plot of a particular ${}_i\sigma_\mu$ is shown in Fig. 4 where ${}_s\sigma_\nu=1$, for all ν. In practice, of course, the errors on the recorded data would not be uniform (e.g., they might depend on the signal intensity as in photoelectric statistics) but the figure gives an indication of the credibility of the final deconvolved intensities. The deconvolved errors can also be used in filtering the deconvolved data by, say, maximum entropy, or likelihood, unfolding techniques. Here the periodicity seen in Fig. 4 re-

flects the 8×8 construction of the detector matrix and the effect of truncated instrument functions at the boundaries.

C. Data reconstruction

The main concern here is to remove interspectra cross talk. Signal spillover between the individual channels in any one spectrum is of less concern as this can be included in making best fits to the data, including the directly measured instrument functions. These latter will include all the smearing effects (e.g., spectrometer finite resolution and focusing effects) and including the cross talk between the detector elements. To avail of the directly measured instrument functions (composite) we first remove the detector element cross talk and then reinsert the cross talk between the spectral channels.

V. EXPERIMENTAL RESULTS

Initial raw data are shown in Fig. 5 from two poloidal views of the COMPASS-D device. The wavelength is 282.2 nm from the heliumlike boron^{3+} impurity. Examples of interpreted data, in terms of velocity and temperature, are shown in Fig. 6 using data from the first of the chords in Fig. 5. The error bars are obtained from a least-squares fit of a single Gaussian spectrum together with a background pedestal and convolved with the measured instrument functions and the Zeeman splitting[17] ($B=1\rightarrow 2T$) of the boron^{3+} transition [$1s2s(S^3)\rightarrow 1s2p(P_2^3)$]. Before fitting to the data, the spatial cross talk is removed as described above. The error bars shown are for time intervals greater than the temporal smearing from the electronics (i.e., when the measurements can be regarded as independent of each other). The small errors in both the ion temperature ($\approx\pm 15$ eV) and velocity ($\approx\pm 0.3$) km s^{-1} show the importance of obtaining good photoelectron statistics for the fast time resolution by having relatively large spectral channels and large spectral dispersion.

ACKNOWLEDGMENTS

Technical assistance from C. A. Bunting and N. J. Conway is greatly appreciated. This work has been funded by the UK Department of Trade and Industry and EURATOM.

[1] T. P. Hughes and A. S. Kaufman, Nature **183**, 7 (1959).
[2] A. A. Ware and J. A. Wesson, Proc. Phys. Soc. London **77**, 801 (1961).
[3] V. I. Bugarya, A. V. Gorshkov, S. A. Grashin, I. V. Ivanov, V. A. Krupin, A. V. Mel'nikov, K. A. Razumova, Yu. A. Sokolov, V. M. Trukhin, V. A. Chankin, P. N. Yushmanov, L. I. Krupnik, and I. S. Nedzel'skij, Nucl. Fusion **25**, 1707 (1985).
[4] N. C. Hawkes and N. J. Peacock, Nucl. Fusion **25**, 971 (1985).
[5] T. C. Hender, R. Fitzpatrick, A. W. Morris, P. G. Carolan, R. D. Durst, T. Edlington, J. Ferreira, S. J. Fielding, P. S. Haynes, J. Hugill, I. J. Jenkins, R. J. La Haye, B. J. Parham, D. C. Robinson, T. N. Todd, M. Valovic, and G. Vayakis, Nucl. Fusion **32**, 2091 (1992).
[6] R. A. Bamford, P. G. Carolan, and C. A. Bunting, Rev. Sci. Instrum. **63**, 4962 (1992).
[7] A. W. Morris, P. G. Carolan, R. Fitzpatrick, T. C. Hender, and T. N. Todd, Phys. Fluids B **4**, 413 (1992).
[8] P. Gohil, K. H. Burrell, E. J. Doyle, R. J. Groebner, L. C. Luhmann, W. A. Peebles, R. Philipona, and R. P. Seraydarian, Proceedings of the 18th EPS Conference on Controlled Fusion and Plasma Physics, Berlin 1991, 15C, I, 289 (1991).
[9] A. R. Field, G. Fussmann, J. V. Hofmann, and the ASDEX-U Team, Nucl. Fusion **32**, 1191 (1992).
[10] P. G. Carolan, S. J. Fielding, S. Gerasimov, J. Hugill, A. W. Morris, D. C. Robinson, T. N. Todd, M. Valovic, J. Ashall, K. B. Axon, R. A. Bamford, C. A. Bunting, T. Edlington, A. M. Edwards, J. G. Ferreira, S. J. Manhood, R. O'Connell, M. A. Singleton, K. Stammers, J. Tomas, D. L. Trotman, and the COMPASS-D Team, Plasma Phys. Control. Fusion **38**, A111 (1994).
[11] T. H. Stix, Phys. Fluids **16**, 1260 (1973).
[12] N. C. Hawkes Proceedings 20th EPS Conference on Controlled Fusion and Plasma Physics, Lisbon 1993, **17C**, I, 3 (1993).
[13] C. A. Bunting, P. G. Carolan, A. R. Field, and M. J. Forrest, Rev. Sci. Instrum. **57**, 2015 (1986).
[14] GP Fibres, Germany.
[15] Haraeus, Silica and Metals Ltd., Germany.
[16] Glen Spectra, interference filter 282BP14.
[17] P. G. Carolan, M. J. Forrest, N. J. Peacock, and D. L. Trotman, Plasma Phys. Controlled Fusion **27**, 1101, (1985).